Design and Evaluation of UAV Flow Angle Estimation Filters

Pengzhi Tian, Haiyang Chao, *Member, IEEE,* Harold Patrick Flanagan, Steven G. Hagerott, Yu Gu, *Member, IEEE*

***Abstract*—This paper presents the design, implementation, and evaluation of four filters for the estimation of angle of attack (AOA) and angle of sideslip (AOS) of small unmanned aerial vehicles (UAVs). Specifically, two novel filters (a complementary filter and an extended Kalman filter) are proposed and evaluated without using direct flow angle and GPS measurements; two existing AOA/AOS filters are also implemented and evaluated. All filters are designed with minimal inputs and states to ensure the ease of implementation, simplicity of tuning, and computation efficiency. Both simulation and UAV flight test results show the performance of the proposed filters. Especially, flight test results from two different UAVs (a T-tail UAV and a flying wing UAV) show that the root mean square errors of estimated inertial AOA and AOS are less than 1.5 degrees under nominal flight conditions and around 2 degrees under aggressive maneuvers compared with direct flow angle measurements.**

***Index Terms*—Flow Angles, Angle of Attack, Angle of Sideslip, Estimation, Extended Kalman Filter, Complementary Filter.**

I. Introduction

Angle of attack (AOA) and angle of sideslip (AOS) (also known as flow angles) describe the interaction between flight vehicles and the surrounding air, which have significant influences on aircraft aerodynamics [1]. Accurate AOA and AOS measurements/estimation are crucial to aircraft model identification and flight control [2], [3]. More importantly, AOA and AOS are flight critical. Pilots rely on AOA for stall warning and for indications of surrounding air flows in order to fly the aircraft efficiently and safely [4], [5]. The malfunction of AOA and AOS sensors could cause severe consequences such as loss of control and catastrophic accidents [6]. Therefore, the redundancy of these signals is usually required for manned aircraft [7]. AOA and AOS measurements are also well accepted as good indicators for turbulence encounters, especially for wake vortex encounters [8], [9]. Recently, AOA and AOS are used for the estimation of 3D wind velocities along the aircraft flight trajectory [10]. For most manned aircraft, AOA and AOS are measured using air flow vanes or multi-hole pressure probes [11]. These sensors are usually mounted ahead of the fuselage nose, ahead of the wing tip, or on the fuselage forebody [12]. It is worth emphasizing that AOA and AOS sensors need to be careful installed and calibrated in order to reduce the influence on local air flows due to the presence of a pitot tube and fuselage [11], [13]. It requires extensive efforts and high costs to achieve desired accuracy, which is often difficult for low-cost small unmanned aerial vehicles (UAVs) [14].

In consideration of redundancy, reliability, accuracy, and cost requirements, different filtering techniques have been proposed for the estimation or reconstruction of AOA and AOS with or without direct flow angle measurements. Based on the sensors used in the filter, these methods fall into two major categories. The first category is to use filters to increase the reliability and accuracy of direct AOA and AOS measurements by removing measurement noises and local flow disturbances [15]–[17]. The second category works without direct flow angle measurements, which can be used either as a redundant/complementary system or as a standalone system. Filters belonging to this category are referred to as inertial AOA/AOS estimation filters [3], [7], [14], [18]–[28]. When direct flow angle measurements are available, filters in the first category are more frequently used for signal quality improvement. An extended Kalman Filter (EKF) is proposed in [15], where the quality of direct flow angle measurements from mechanical vanes is improved with the help from global positioning system (GPS) and inertial measurement unit (IMU) data. Besides Kalman filters, complementary filters (CFs) can also be used to filter out noises and local flow disturbances from direct flow angle measurements [16], [17].

For the second category, without direct flow angle measurements, inertial AOA and AOS can be estimated mainly based on inertial measurements of aircraft dynamic responses to the surrounding flow. Inertial AOA and AOS can be calculated by integrating inertial data over time, however, the direct integration method usually suffers from nontrivial biases and drifts [14]. To solve this problem, different filtering techniques can be applied, including CFs [22], [29] and Kalman filters [7], [18]–[21], [23]–[28]. Among these methods, [23], [27], [28] are able to estimate flow angles without relying on aircraft aerodynamic models by correlating airspeed measurements with GPS ground speed measurements using wind triangle equations. When airspeed measurements and partial aircraft aerodynamic model parameters are available, flow angles can be estimated without GPS measurements [7], [18]–[21], [29]. For cases when the more sophisticated aircraft model is available, even airspeed measurements are not required [26]. From aforementioned literature, it can be observed that studies on flow angle estimation often have strong correlations with wind estimation problems [10], [15], [19], [22], [25]–[30]. There are also several other approaches for inertial flow angle estimation. A frequency domain system identification method is proposed in [14], where flow angles are first reconstructed in the time domain and then transformed into frequency domain to eliminate integration biases and drifts. An alternative method to assist aircraft system identification is called flight path reconstruction (FPR). For this technique, AOA and AOS are reconstructed by integrating inertial data using an output error minimization method [3]. It is also possible to estimate inertial AOA and AOS by using algorithms such as the Newton-Raphson solver [24]. However, these optimization methods are not suitable for real time applications due to their high

Ph.D. Student, Aerospace Engineering Department, University of Kansas, Lawrence, KS, 66045. E-mail: pengzhitian@ku.edu.

Assistant Professor, Aerospace Engineering Department, University of Kansas, Lawrence, KS, 66045. E-mail: chaohaiyang@ku.edu.

Ph.D. Student, Aerospace Engineering Department, University of Kansas, Lawrence, KS, 66045. E-mail: h682f304@ku.edu.

Sr. Engineering Specialist, Textron Aviation, Wichita, KS, 67235. E-mail: shagerott@txtav.com

Associate Professor, Mechanical & Aerospace Engineering Department, West Virginia University, Morgantown, WV, 26506. E-mail: Yu.Gu@mail.wvu.edu.

demands on computational power.

In summary, most of the existing methods for flow angle estimation either require direct flow angle sensors, GPS measurements, or sophisticated aircraft dynamic models, which can be difficult for small UAV applications. These difficulties and logistic challenges led to few flight test validation results on UAVs. This paper is focused on increasing the redundancy and reliability as well as reducing the cost of flow angle systems. It is a significant extension of our previous work [31], where only the filters that require direct flow angle measurements are implemented and tested on one UAV platform (Phastball). In this paper, four AOA and AOS estimation filters are designed, implemented, and evaluated on two UAV platforms (Phastball and KHawk 55"), including two new filters (1 EKF and 1 CF) for inertial flow angle estimation without using direct flow angle measurements and two existing filters (1 EKF and 1 CF [31]) for noise removal of direct flow angle measurements. All filters are formed with minimal inputs and states to ensure the ease of implementation, simplicity of tuning, and computational efficiency. Especially, the proposed inertial flow angle estimation filters can work as an independent and redundant unit on small UAVs to improve UAV safety and flight performance as well as facilitate studies on wind estimation and turbulence sensing. In addition, GPS measurements are not required for filters designed in this paper, which is convenient for small UAVs that operate under GPS degraded or denied environments. The major contributions of this paper can be summarized as follows:

1) To reduce the dependency in direct flow measurement systems, two novel filters (a CF and an EKF based designs) are proposed and evaluated on a T-tail UAV (Phastball) and a flying wing UAV (KHawk 55"), where inertial AOA and AOS are estimated without using direct flow angle measurements and GPS measurements;
2) Flight test evaluation of all four filters are conducted on two different UAV platforms under nominal flight conditions and aggressive maneuvers. Filter formulation and tuning procedures are discussed and compared in detail.

The organization of this paper can be summarized as follows. The problem of AOA and AOS estimation is formulated in Section II. Then, four fusion algorithms are introduced in detail in Section III. Simulation and flight test results are presented in Section IV and Section V, respectively. Finally, conclusions are made in Section VI.

II. Problem Formulation

Angle of attack (AOA or α) is defined as the angle between a reference line on the aircraft and the flight direction [32], shown in Fig. 1, where V is the airspeed and $[u, v, w]$ are airspeed projections in aircraft body-axis. The reference line is usually chosen as the chord line of an airfoil [32] and an AOA relative to this line is called the geometric angle of attack [33]. Similarly, sideslip angle (AOS or β) is defined as the angle between the x-z plane in the body frame of the aircraft and the incoming flow [34].

AOA and AOS can be directly measured using air flow sensors installed on an aircraft. Typical air flow sensors are flow vanes and multi-hole pitot tubes. A flow vane, also known as a pivoted vane, is a mass-balanced wind vane that can align itself with the direction of the incoming air flow [11]. The angle between a flow vane and the reference line on the aircraft can then be measured by a potentiometer. Multi-hole pitot tubes can measure flow angles by sensing the pressure difference from different holes [11]. There also exist other direct measurement methods. Differential pressure probes can be used to measure AOA when calibration and normalization is properly done [35]. Distributed flush airdata systems are another solution [36]. It is also possible to measure flow angles by using optical sensors [37]. It is worth mentioning that direct flow measurements are usually corrupted by noises.

AOA and AOS can also be estimated, or reconstructed using measurements mainly from inertial sensors, which are called inertial AOA and AOS. A typical method for inertial AOA and AOS reconstruction is to combine measurements from the pitot tube (V_{pitot}), accelerometers (a_x, a_y, a_z), and gyroscopes (p, q, r). Inertial AOA/AOS and measured AOA/AOS usually match with each other in a calm atmosphere. However, they may show non-trivial difference in dynamic flow fields due to effects caused by local turbulence [8], [38].

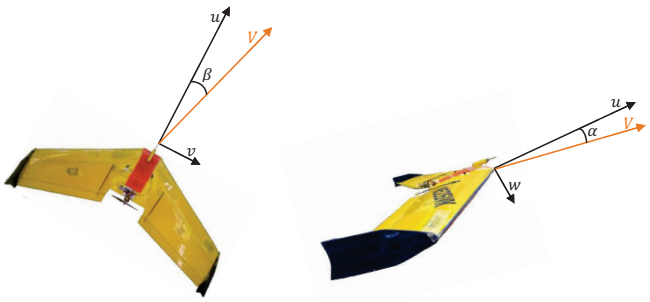

Fig. 1. of AOA and AOS.

This paper exploits the AOA/AOS measurement and estimation methods. Two types of filters are designed, implemented, and evaluated for AOA/AOS estimation. Direct AOA/AOS measurements from mechanical vanes or a multi-hole pitot tube are used as the ground truth for validation purpose. Based on sensor and aircraft model availability, filters studied in this paper can be categorized into two types:

1) For aircraft with low quality AOA/AOS sensors such as custom-made flow vanes, a CF and an EKF are developed for the noise rejection with the help of inertial measurements and pitot tube measured airspeed;
2) For aircraft without direct flow angle sensors, a simple model aided CF and a simple model aided EKF are designed for inertial AOA/AOS estimation with the help of inertial measurements, pitot tube measured airspeed, and pre-identified aircraft lift and side force coefficients.

III. Sensor Fusion Algorithms

In this section, algorithms used for AOA and AOS estimation are presented. To ensure the ease of implementation, simplicity of tuning, and computational efficiency, all filters are designed in the most compact form for the estimation of both AOA and AOS.

A. Extended Kalman Filter for AOA and AOS Estimation

EKF is one of the most commonly used algorithms for combining measurements from multiple noisy sensors [39], [40]. Given corrupted measurements from GPS (optional), IMU, and flow sensors, one approach is to estimate the body-frame velocity components (u, v, w) first and then calculate AOA and AOS based on the estimated velocity components. The other approach is directly using AOA and AOS (α, β) as EKF states. In this paper, both EKF formulations are implemented and evaluated.

1) EKF: Filtering of Direct Flow Angle Measurements: This filter was proposed in our former work [31], which can filter direct AOA/AOS measurements without relying on GPS measurements. In this approach, IMU measurements $[a_x, a_y, a_z, p, q, r]$, airspeed measurement $[V_{pitot}]$, flow vane measurements $[\alpha_m, \beta_m]$, and aircraft attitude $[\phi, \theta]$ are assumed to be available. $[u, v, w]$ are used as systems states for the EKF. The propagation equation of this EKF is derived from equations of translational motion of an aircraft [3],

$$\begin{bmatrix} \dot{u} \\ \dot{v} \\ \dot{w} \end{bmatrix} = \begin{bmatrix} -qw + rv - g\sin\theta + a_x \\ -ru + pw - g\cos\theta\sin\phi + a_y \\ -pv + qu - g\cos\theta\cos\phi + a_z \end{bmatrix}. \quad (1)$$

The update equation is given by the relation between $[u, v, w]$ and $[V, \alpha, \beta]$ as follows

$$\begin{bmatrix} V \\ \alpha \\ \beta \end{bmatrix} = \begin{bmatrix} \sqrt{u^2+v^2+w^2} \\ \tan^{-1}(\frac{w}{u}) \\ \sin^{-1}(\frac{v}{V}) \end{bmatrix}. \quad (2)$$

The noises are considered for both the system inputs and observations. For such a model, the state $\mathbf{x}$, input $\mathbf{u}$, non-linear measurement function $\mathbf{h}$, and measurement $\mathbf{z}$ vectors are given by

$$\mathbf{x} = [u\ v\ w]^T \quad (3a)$$

$$\mathbf{u} = [a_x\ a_y\ a_z\ p\ q\ r\ \phi\ \theta]^T \quad (3b)$$

$$\mathbf{h}(\mathbf{x}, \mathbf{u}, \mathbf{0}) = [\sqrt{u^2+v^2+w^2}\ \tan^{-1}(\frac{w}{u})\ \sin^{-1}(\frac{v}{V})]^T \quad (3c)$$

$$\mathbf{z} = \mathbf{h}(\mathbf{x}, \mathbf{u}, \mathbf{v}) = [V_m\ \alpha_m\ \beta_m]^T \quad (3d)$$

where m denotes measured data and $\mathbf{v}$ is the measurement noise vector.

2) EKF: Inertial AOA/AOS Estimation: In this approach, IMU measurements $[a_x, a_y, a_z, p, q, r]$, airspeed measurement $[V_{pitot}]$, aircraft attitude $[\phi, \theta]$, control surface deflections $[\delta_e, \delta_a, \delta_r]$, aircraft lift coefficients $[C_{L_0}, C_{L_\alpha}, C_{L_q}, C_{L_{\delta_e}}]$, and side force coefficients $[C_{Y_0}, C_{Y_\beta}, C_{Y_p}, C_{Y_r}, C_{Y_{\delta_a}}, C_{Y_{\delta_r}}]$ are assumed to be available. $[\alpha, \beta]$ are used as systems states for the EKF. The propagation equations of this EKF, shown in Eqs.

$$\dot{\alpha} = q - (p\cos\alpha + r\sin\alpha)\tan\beta + \frac{g(\cos\phi\cos\theta\cos\alpha + \sin\theta\sin\alpha) - a_x\sin\alpha + a_z\cos\alpha}{V\cos\beta} \quad (4)$$

$$\dot{\beta} = \frac{1}{V}[-a_x\cos\alpha\sin\beta + a_y\cos\beta - a_z\sin\alpha\sin\beta + g(\sin\theta\cos\alpha\sin\beta + \cos\theta\sin\phi\cos\beta - \cos\theta\cos\phi\sin\alpha\sin\beta)] + p\sin\alpha - r\cos\alpha \quad (5)$$

The update equations are shown in Eqs. (6) and (7), which can be derived from aircraft lift and side force equations. Detailed derivations can be found in Eqs. (8)-(10).

$$C_{L_0} + \frac{C_{L_q}q\bar{c}}{2V} + C_{L_{\delta_e}}\delta_e = \frac{m(a_x\sin\alpha - a_z\cos\alpha)}{\bar{q}S} - C_{L_\alpha}\alpha \quad (6)$$

$$\frac{1}{C_{Y_\beta}}(\frac{ma_y}{\bar{q}S} - C_{Y_0} - \frac{C_{Y_p}pb}{2V} - \frac{C_{Y_r}rb}{2V} - C_{Y_{\delta_a}}\delta_a - C_{Y_{\delta_r}}\delta_r) = \beta \quad (7)$$

where b is the wingspan, $\bar{c}$ is the mean chord length, S is the wing area, and $\bar{q}$ is the dynamic pressure.

According to the aircraft force equation, lift can be expressed as the projection of thrust and body-axis accelerations. Note that the thrust projection is much smaller than the lift during normal flight conditions, therefore, it can be removed for simplification.

$$L = m(a_x\sin\alpha - a_z\cos\alpha) - T\sin\alpha \approx m(a_x\sin\alpha - a_z\cos\alpha) \quad (8)$$

Lift can also be approximated as

$$L = C_L\bar{q}S \approx (C_{L_0} + C_{L_\alpha}\alpha + C_{L_{\delta_e}}\delta_e + C_{L_q}q\bar{c}/(2V))\bar{q}S. \quad (9)$$

By substituting lift from Eq. (9) in Eq. (8) and moving terms that contain α to the right side of equation, Eq. (6) is derived.

Similarly, Eq. (7) can be derived by correlating side force equations, shown in Eq. (10), and moving terms that contain β to the right side of equation.

$$Y = ma_y = C_Y\bar{q}S \approx (C_{Y_0} + C_{Y_\beta}\beta + \frac{C_{Y_p}pb}{2V} + \frac{C_{Y_r}rb}{2V} + C_{Y_{\delta_a}}\delta_a + C_{Y_{\delta_r}}\delta_r)\bar{q}S \quad (10)$$

The main philosophy behind the update equations is that the lift and side forces of the aircraft can be estimated from the accelerometer readings, and the long-term error is quite small around the trim point during steady state wings-level flight.

The state $\mathbf{x}$, input $\mathbf{u}$, non-linear measurement function $\mathbf{h}$, and measurement $\mathbf{z}$ vectors for this filter are given by

$$\mathbf{x} = [\alpha\ \beta]^T \quad (11a)$$

$$\mathbf{u} = [a_x\ a_y\ a_z\ p\ q\ r\ \phi\ \theta\ V]^T \quad (11b)$$

$$\mathbf{h}(\mathbf{x}, \mathbf{u}, \mathbf{0}) = \begin{bmatrix} m(a_x\sin\alpha - a_z\cos\alpha)/(\bar{q}S) - C_{L_\alpha}\alpha \\ \beta \end{bmatrix} \quad (11c)$$

$$\mathbf{z} = \mathbf{h}(\mathbf{x}, \mathbf{u}, \mathbf{v}) = \begin{bmatrix} C_{L_0} + \frac{C_{L_q} q\bar{c}}{2V} + C_{L_{\delta_e}} \delta_e \\ \frac{1}{C_{Y_\beta}} (\frac{ma_y}{\bar{q}S} - C_{Y_0} - \frac{C_{Y_p} pb}{2V} - \frac{C_{Y_r} rb}{2V} - C_{Y_{\delta_a}} \delta_a - C_{Y_{\delta_r}} \delta_r) \end{bmatrix} \quad (11)$$

3) EKF Process: This paper follows the EKF process described in [41]. The nonlinear discrete state space model is given by

$$\mathbf{x}_k = f(\mathbf{x}_{k-1}, \mathbf{u}_{k-1}, \mathbf{w}_{k-1}) \quad (12)$$

$$\mathbf{z}_k = h(\mathbf{x}_k, \mathbf{u}_k, \mathbf{v}_k) \quad (13)$$

where f is the non-linear state function, $\mathbf{w}_k$ and $\mathbf{v}_k$ are random variables that represent the process and measurement noise.

The EKF time update equations are given as

$$\hat{\mathbf{x}}_k^- = f(\hat{\mathbf{x}}_{k-1}, \mathbf{u}_{k-1}, \mathbf{0}) \quad (14)$$

$$\mathbf{P}_k^- = \mathbf{A}_k \mathbf{P}_{k-1} \mathbf{A}_k^T + \mathbf{W}_k \mathbf{Q}_{k-1} \mathbf{W}_k^T \quad (15)$$

where EKF measurement update equations are given as

$$\mathbf{K}_k = \mathbf{P}_k^- \mathbf{H}_k^T (\mathbf{H}_k \mathbf{P}_k^- \mathbf{H}_k^T + \mathbf{R}_k) \quad (16)$$

$$\hat{\mathbf{x}}_k = \hat{\mathbf{x}}_k^- + \mathbf{K}_k (\mathbf{z}_k - h(\hat{\mathbf{x}}_k^-, \mathbf{u}_k, \mathbf{0})) \quad (17)$$

$$\mathbf{P}_k = (\mathbf{I} - \mathbf{K}_k \mathbf{H}_k) \mathbf{P}_k^-. \quad (18)$$

$\mathbf{A}$, $\mathbf{W}$, and $\mathbf{H}$ are Jacobian matrices that can be calculated by

$$\mathbf{A}_{[i,j]} = \frac{\partial f_{[i]}}{\partial x_{[j]}} (\hat{\mathbf{x}}_{k-1}, \mathbf{u}_{k-1}, \mathbf{0}) \quad (19)$$

$$\mathbf{W}_{[i,j]} = \frac{\partial f_{[i]}}{\partial w_{[j]}} (\hat{\mathbf{x}}_{k-1}, \mathbf{u}_{k-1}, \mathbf{0}) \quad (20)$$

$$\mathbf{H}_{[i,j]} = \frac{\partial h_{[i]}}{\partial x_{[j]}} (\hat{\mathbf{x}}_k^-, \mathbf{u}_{k-1}, \mathbf{0}). \quad (21)$$

The EKF tuning process is discussed in Section V, which includes the selection of initial covariance $\mathbf{P}_0$, process noise covariance $\mathbf{Q}$, and measurement noise covariance $\mathbf{R}$.

B. Complementary Filter for AOA and AOS Estimation

The complementary filter is another approach to reconstruct AOA and AOS. The CF generally consists of two parts, a second-order low pass filter and a second-order high pass filter, which can increase the system's bandwidth.

1) CF: Filtering of Direct Flow Angle Measurements: This filter was mainly used on manned aircraft to filter out the noise from flow vane or conventional probe measurements [16], [17]. In this approach, IMU measurements [a_x, a_y, a_z, p, q, r], airspeed measurement [V_{pitot}], flow vane measurements [α_m, β_m], and aircraft attitude [ϕ, θ] are assumed to be available.

AOA and AOS can be reconstructed by the combinations of the high-frequency portions of $\dot{\alpha}/\dot{\beta}$ and the low-frequency portions of flow vane measurements α_m/β_m, shown in Eqs. (22) and (23) [16], [17]

$$\alpha_{cf\_filtered} = \underbrace{\frac{s}{s^2 + 2\zeta_{cf}\omega_{n_{cf}} s + {\omega_{n_{cf}}}^2} \dot{\alpha}}_{\text{High Frequency Contribution}} + \underbrace{\frac{2\zeta_{cf}\omega_{n_{cf}} s + {\omega_{n_{cf}}}^2}{s^2 + 2\zeta_{cf}\omega_{n_{cf}} s + {\omega_{n_{cf}}}^2} \alpha_m}_{\text{Low Frequency Contribution}} \quad (22)$$

$$\beta_{cf\_filtered} = \underbrace{\frac{s}{s^2 + 2\zeta_{cf}\omega_{n_{cf}} s + {\omega_{n_{cf}}}^2} \dot{\beta}}_{\text{High Frequency Contribution}} + \underbrace{\frac{2\zeta_{cf}\omega_{n_{cf}} s + {\omega_{n_{cf}}}^2}{s^2 + 2\zeta_{cf}\omega_{n_{cf}} s + {\omega_{n_{cf}}}^2} \beta_m}_{\text{Low Frequency Contribution}} \quad (23)$$

where ζ_{cf} is the filter damping ratio and $\omega_{n_{cf}}$ is the break frequency of the complementary filter. $\dot{\alpha}$ and $\dot{\beta}$ are calculated from Eqs. (4) and (5). α_m and β_m are measurements from mechanical vanes which usually contain high frequency noise.

2) CF: Inertial AOA/AOS Estimation: This filter is similar to [22], however, given the fact that the low-cost GPS receivers on most UAVs cannot provide accurate flight path angle under dynamic maneuvers, alternative measurements and equations are used. In this approach, IMU measurements [a_x, a_y, a_z, p, q, r], airspeed measurement [V_{pitot}], aircraft attitude [α, β], control surface deflections [$\delta_e, \delta_a, \delta_r$], aircraft lift coefficients [$C_{L_0}, C_{L_\alpha}, C_{L_q}, C_{L_{\delta_e}}$], and side force coefficients [$C_{Y_0}, C_{Y_\beta}, C_{Y_p}, C_{Y_r}, C_{Y_{\delta_a}}, C_{Y_{\delta_r}}$] are assumed to be available.

Reconstructed AOA and AOS can be calculated by Eqs. (24) and (25).

$$\alpha_{cf\_inertial} = \underbrace{\frac{s}{s^2 + 2\zeta_{cf}\omega_{n_{cf}} s + {\omega_{n_{cf}}}^2} \dot{\alpha}}_{\text{High Frequency Contribution}} + \underbrace{\frac{2\zeta_{cf}\omega_{n_{cf}} s + {\omega_{n_{cf}}}^2}{s^2 + 2\zeta_{cf}\omega_{n_{cf}} s + {\omega_{n_{cf}}}^2} \alpha_{long}}_{\text{Low Frequency Contribution}} \quad (24)$$

$$\beta_{cf\_inertial} = \underbrace{\frac{s}{s^2 + 2\zeta_{cf}\omega_{n_{cf}} s + {\omega_{n_{cf}}}^2} \dot{\beta}}_{\text{High Frequency Contribution}} + \underbrace{\frac{2\zeta_{cf}\omega_{n_{cf}} s + {\omega_{n_{cf}}}^2}{s^2 + 2\zeta_{cf}\omega_{n_{cf}} s + {\omega_{n_{cf}}}^2} \beta_{long}}_{\text{Low Frequency Contribution}} \quad (25)$$

$\dot{\alpha}$ and $\dot{\beta}$ are calculated by using Eqs. (4) and (5). α_{long} and β_{long} are calculated based from Eqs. (6) and (7) by moving α and β to the left side of equation, shown in Eqs. (26) and (27).

$$\alpha_{long} = \frac{m(a_x \sin\alpha - a_z \cos\alpha)/\bar{q}S - C_{L_0} - C_{L_q} q\bar{c}/2V - C_{L_{\delta_e}}\delta_e}{C_{L_\alpha}} \tag{26}$$

$$\beta_{long} = \frac{1}{C_{Y_\beta}}\left(\frac{ma_y}{\bar{q}S} - C_{Y_0} - \frac{C_{Y_p} pb}{2V} - \frac{C_{Y_r} rb}{2V} - C_{Y_{\delta_a}}\delta_a - C_{Y_{\delta_r}}\delta_r\right) \tag{27}$$

The AOA and AOS reconstructed from this complementary filter are combinations of the high-frequency portions of $\dot{\alpha}/\dot{\beta}$ and the low-frequency portions of $\alpha_{long}/\beta_{long}$. Note that in implementation the α on the right side of Eq. (26) is approximated by $\alpha_{cf\_inertial}$ estimated from the previous time step.

IV. Simulation Results

Simulation results are focused in this section for the validation of fusion algorithms described in Section III. The WVU Phastball UAV simulator was used, which is based on MATLAB Flight Dynamics and Control (FDC) toolbox. More details can be found in [42].

During the simulation, elevator and aileron doublet inputs were used to excite changes in α and β. The input commands and aircraft states are shown in Fig. 2. Gaussian noises were added to measured aircraft states based on noise characteristics from real sensors [43]. It can be observed from Fig. 2 that there is an elevator doublet at around 10 seconds and an aileron doublet at around 12 seconds. AOA and AOS induced by doublet maneuvers are shown in Fig. 3 and Fig. 4, including noisy measurements, ground truth, and estimation results.

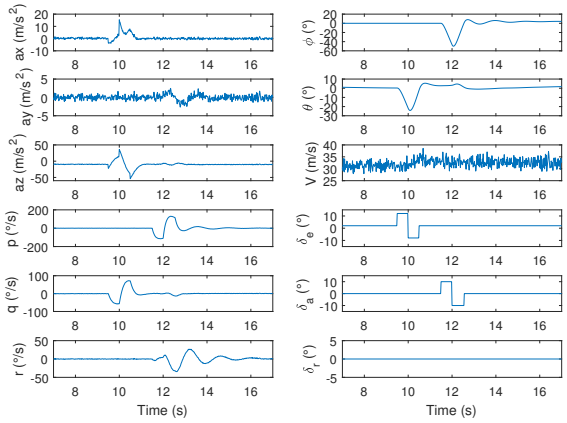

Fig. 2. Aircraft states during doublet maneuvers.

The means and standard deviations of the absolute estimation errors using different algorithms are calculated and

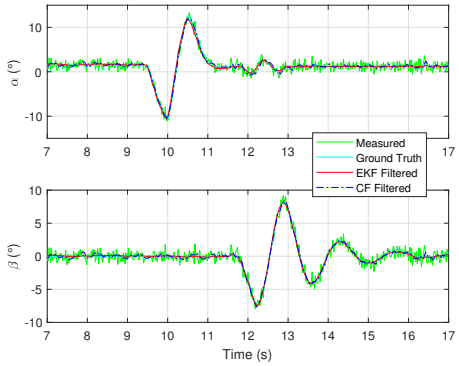

Fig. 3. Filtered α/β vs. ground truth during doublet maneuvers.

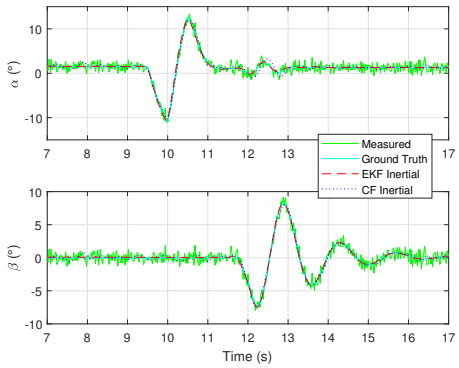

Fig. 4. Estimated inertial α/β vs. ground truth during doublet maneuvers.

provided in Table I. The statistics table shows that all four filters can estimate AOA and AOS accurately. EKFs perform better than CF because all sensor noises are considered in the equations. Inertial AOA and AOS methods show better performance than AOA/AOS filtering methods. This is because in simulation, aircraft lift and side force coefficients are perfectly known and no turbulence is considered. It is worth mentioning that EKFs require more tuning efforts compared with CFs, given the fact that there are only two parameters to tune for CFs and more than ten parameters to tune for EKFs. CFs are also more computationally efficient than EKF. Detailed tuning strategies for both CFs and EKFs will be explained in the following section.

V. UAV Flight Test Evaluation

A. Experimental Platforms

A Phastball UAV with flow vanes and a KHawk 55" UAV with a 5-hole pitot tube, shown in Fig. 5 and Fig. 6, are used for flight evaluation of designed filters. General specifications of the UAVs are shown in Table II.

Custom designed avionics were installed on a Phastball UAV to collect data from sensors including GPS, IMU, range sensor, etc. An ADIS-16405 MEMS (micro-electro-mechanical systems) IMU was used to measure the rotation rates and the linear accelerations. An EKF was running on an 800 MHz general-purpose computer (PC104) to provide real

TABLE I
SIMULATED AOA/AOS ESTIMATION RESULTS DURING DOUBLET MANEUVERS (7S - 17S)

Method	AOA mean error (°)	AOA error std. (°)	AOS mean error (°)	AOS error std. (°)
CF Filtered	0.2733	0.2108	0.1945	0.1518
EKF Filtered	0.1790	0.1748	0.0872	0.0771
CF Inertial	0.2531	0.2034	0.1896	0.1344
EKF Inertial	0.0961	0.1684	0.0744	0.0721

TABLE II
SPECIFICATIONS OF PHASTBALL AND KHAWK 55" UAVS

UAV Parameters	Phastball	KHawk 55"
Take-off Weight	11.2 kg	2.5 kg
Max Payload	3.2 kg	0.5 kg
Wingspan	2.4 m	1.4 m
Mean Chord Length	0.33 m	0.38 m
Wing Area	0.73 m^2	0.5 m^2
Control Surfaces	Ailerons/Elevators/Rudder	Elevons
Engine	Electric Ducted Fans	Pusher Motor
Endurance	$\sim$ 5 minutes	$\sim$ 45 minutes
Cruise Speed	30 m/s	20 m/s
Take-off	Asphalt Runway	Bungee

time attitude estimation, with a typical error of less than 2 degrees for pitch and roll angles under dynamic circumstances [44]. Flight data were also collected from two angle of attack vanes and one sideslip vane attached to potentiometers with a 10 Volts analog to digital converter at 16-bit resolution, shown in Fig. 5. A pitot tube was mounted on the nose boom of the aircraft along the longitudinal axis. The signals were sampled at 50 Hz.

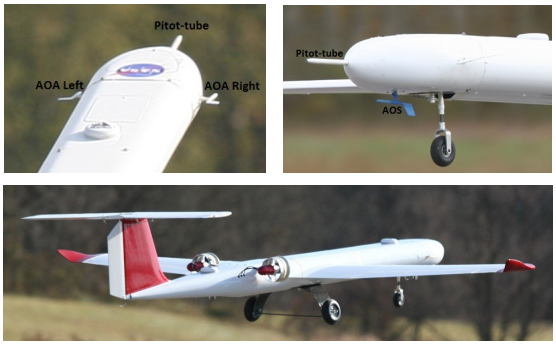

Fig. 5. Phastball UAV platform.

The KHawk 55" UAS supports both manual remote controlled mode and autonomous mode. The airborne avionics includes a Microstrain GX3-25 IMU, a u-blox GPS receiver, a 900 MHz data modem, a Gumstix computer, an open source Paparazzi autopilot, and a manufacturer calibrated Aeroprobe 5-hole air data system (ADS). The 5-hole pitot tube setup is shown in the right of Fig. 6. All sensor data are logged onboard the aircraft including inertial data (100 Hz), GPS data (4 Hz), and air data (100 Hz). The Microstrain GX3-25 IMU on KHawk 55" UAV can provide attitude estimates with a static accuracy of ± 0.5 degrees and a typical dynamic accuracy of ± 2 degrees for attitude estimation, based on the manufacturer [45]. It is worth mentioning that the Aeroprobe 5-hole pitot tube has an airspeed range of 8 to 45 m/s and AOA/AOS range of -20 to 20 degrees. In other words, the Aeroprobe pitot tube will not report a valid measurement when operating outside of the calibrated range.

Fig. 6. KHawk 55" UAV platform.

The lift and side force coefficients of Phastball and KHawk 55" are shown in Table III. The Phastball coefficients were identified from previous flight tests [46], shown in the top of Table III. The flight data were collected during nominal flight conditions with elevator, aileron, and rudder doublet maneuvers. The KHawk 55" coefficients were identified from flight tests using the least squares method [47], shown in the bottom of Table III.

B. Filter Implementation and Tuning for Flight Test

This section summarizes and discusses the filter implementation and tuning process for flight test data.

During the filter implementation process, the locations of sensors and characteristics of sensors need to be carefully considered. For example, if the IMU is not installed at the center of gravity of an aircraft, lever arm and calibration might be required for all IMU measurements [3]. Sensor characteristics including the IMU and airspeed sensor are also critical. IMU measurements are known to have bias errors, which need to be removed to achieve better estimation results. In this paper, the IMU biases are assumed to be provided by navigation systems, which is the case for many commercial, custom-made, and open source autopilots and IMUs. For example, the Phastball UAV has a 15-state EKF running on board for the estimation of aircraft attitude and accelerometer/gyroscope biases [40]. The Microstrain GX3-25 IMU used on KHawk 55" also provides real-time IMU bias estimates [48]. With the availability of this information, biases can be removed from IMU measurements before passing them to the AOA/AOS estimation filters.

Also note that for different types of pitot tubes with varying nose shapes and impact openings, the conversion equation from differential pressure to airspeed may be different due to effects from inclination angles [49]. Many pitot tubes used on small UAVs are small-bore cylindrical tubes, which are

TABLE III
LIFT AND SIDE FORCE COEFFICIENTS OF PHASTBALL (TOP) AND KHAWK 55" (BOTTOM) UAVS

C_{L_0}	$C_{L_\alpha}(rad^{-1})$	$C_{L_q}(s/rad)$	$C_{L_{\delta_e}}(rad^{-1})$	C_{Y_0}	$C_{Y_\beta}(rad^{-1})$	$C_{Y_p}(s/rad)$	$C_{Y_r}(s/rad)$	$C_{Y_{\delta_a}}(rad^{-1})$	$C_{Y_{\delta_r}}(rad^{-1})$
0.1	3.309	41.937	1.787	0	-0.271	0	0.058	0	0.045
0.0563	1.8789	0.1796	0.8297	0.0037	-0.25	0.0065	0.0123	0.0351	NA

insensitive to inclination angles with a range of ± 12 degrees [49]. Therefore, the following equation is used in this paper.

$$V_{pitot} = V \tag{28}$$

Pitot tubes are usually mounted along the longitudinal axis of an aircraft. Thus, for pitot tubes that are sensitive to inclination angles, only the projection of the true airspeed in the body x-axis can be measured. The simple output equation can be used [15]

$$V_{pitot} = u \tag{29}$$

instead of V in Eq. (2). The true airspeed V needs to be expressed using pitot tube airspeed V_{pitot}, given as:

$$V = \frac{V_{pitot}}{\cos\alpha\cos\beta} \tag{30}$$

The tuning of CF is relatively simple with only two parameters, ζ_{cf} and $\omega_{n_{cf}}$, to tune. These two parameters determine the frequency response and bandwidth of the filter. The CF damping ratio ζ_{cf} is selected as 0.7 in this paper, considering typical dynamic responses of a second order system. The filter frequency $\omega_{n_{cf}}$ is selected as 10 rad/s, which is close to the short period frequency of small UAVs used in this paper.

The tuning process of the EKF for flight tests can be tedious since more parameters are involved. In this paper, some of process noises and measurement noises with physical meanings are determined through experiments, while others are manually tuned. For example, IMU measurement noises are determined from ground tests [43]. By doing this, the EKF tuning load is significantly reduced. Detailed EKF tuning parameters used for Phastball and KHawk 55" are shown in Table IV. Note that the process noise covariance $\mathbf{Q}$ (corresponding to the input vector $\mathbf{u}$), and measurement noise covariance $\mathbf{R}$ (corresponding to the observation vector $\mathbf{z}$) are assumed to be diagonal. The initial covariance $\mathbf{P}_0$ (corresponding to the state vector $\mathbf{x}$) is assumed to be an identity matrix in this paper.

C. Results of Flight Test Evaluation

Based on the availability of sensors and aircraft model parameters, corresponding filters are evaluated on both the Phastball and KHawk 55" UAS platforms.

All four fusion algorithms are compared using the Phastball UAV's flight data, where IMU measurements $[a_x, a_y, a_z]$ $[p, q, r]$, airspeed measurement $[V_{pitot}]$, flow vane measurements $[\alpha, \beta]$, aircraft attitude $[\phi, \theta]$, aircraft lift coefficients $[C_{L_0}, C_{L_\alpha}, C_{L_q}, C_{L_{\delta_e}}]$, and side force coefficients $[C_{Y_0}, C_{Y_\beta}, C_{Y_p}, C_{Y_r}, C_{Y_{\delta_a}}, C_{Y_{\delta_r}}]$ are available.

The CF filtered AOA and AOS are compared with flow vane measurements, shown in Fig. 7. The enlarged results for doublet maneuvers are shown in Fig. 8. It can be observed that the CF filtered out high frequency noise from raw flow angle measurements. On manned aircraft, noisy flow vane measurements are typically filtered by a CF and then used for stall warnings or control purposes [16], [20]. Similar approaches can be used on UAVs. The EKF filtered AOA and AOS are shown in Fig. 9 and Fig. 10 (enlarged). It can be observed that the EKF also filters out high frequency noise in flow angle measurements.

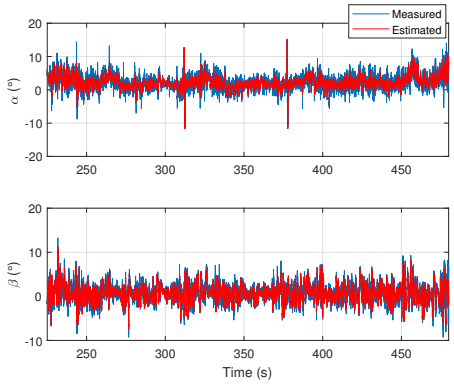

Fig. 7. Phastball CF filtered results vs. flow vane measurements.

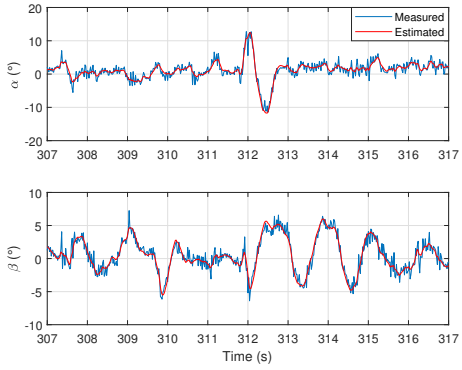

Fig. 8. Phastball CF filtered results vs. flow vane measurements (enlarged).

Inertial AOA and AOS estimation using the CF and EKF are further presented in Figs. 11-14. Inertial AOA and AOS are especially useful for cases where direct flow angle measurements are not available, such as low cost UAVs and hypersonic aircraft. They can also be used for the detection of turbulence encounters when compared with direct flow angle measurements [8], [38].

Statistical analysis of estimation results from two inertial filters are provided in Table V. The flow vane measurements

TABLE IV
EKF TUNING PARAMETERS FOR PHASTBALL AND KHAWK 55" UAVS

Phastball AOA/AOS Filtering EKF		Phastball Inertial EKF		KHawk 55" Inertial EKF	
Process Noise $\mathbf{Q}$	Measurement Noise $\mathbf{R}$	Process Noise $\mathbf{Q}$	Measurement Noise $\mathbf{R}$	Process Noise $\mathbf{Q}$	Measurement Noise $\mathbf{R}$
$0.02889^2\ (m/s^2)^2$	$1\ (m/s)^2$	$0.02889^2\ (m/s^2)^2$	$10^{-7}\ (rad/s)^2$	$0.01366^2\ (m/s^2)^2$	$10^{-7}\ (rad/s)^2$
$0.02899^2\ (m/s^2)^2$	$4 \times 10^{-4}\ (rad/s)^2$	$0.02899^2\ (m/s^2)^2$	$10^{-5}\ (rad/s)^2$	$0.01819^2\ (m/s^2)^2$	$10^{-7}\ (rad/s)^2$
$0.02471^2\ (m/s^2)^2$	$4 \times 10^{-4}\ (rad/s)^2$	$0.02471^2\ (m/s^2)^2$		$0.02007^2\ (m/s^2)^2$	
$0.00376^2\ (rad/s)^2$		$0.00376^2\ (rad/s)^2$		$0.00251^2\ (rad/s)^2$	
$0.00468^2\ (rad/s)^2$		$0.00468^2\ (rad/s)^2$		$0.00309^2\ (rad/s)^2$	
$0.00413^2\ (rad/s)^2$		$0.00413^2\ (rad/s)^2$		$0.00266^2\ (rad/s)^2$	
$10^{-7}\ (rad/s)^2$		$10^{-7}\ (rad/s)^2$		$10^{-7}\ (rad/s)^2$	
$10^{-7}\ (rad/s)^2$		$10^{-7}\ (rad/s)^2$		$10^{-7}\ (rad/s)^2$	
		$1\ (m/s)^2$		$0.25\ (m/s)^2$	

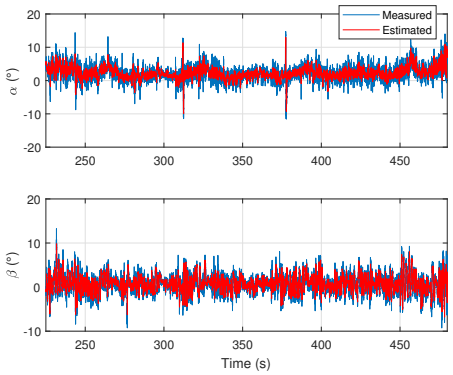

Fig. 9. Phastball EKF filtered results vs. flow vane measurements.

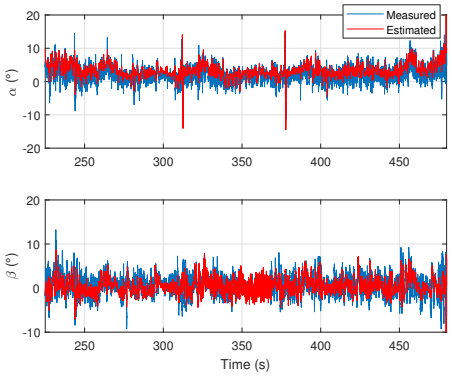

Fig. 11. Phastball CF inertial results vs. flow vane measurements.

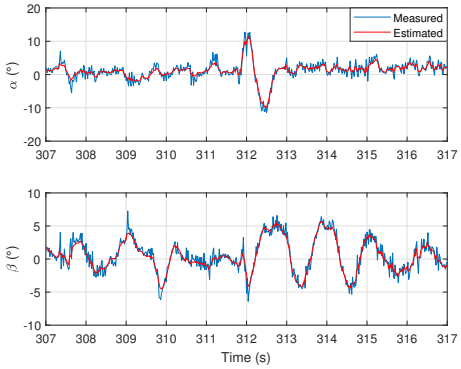

Fig. 10. Phastball EKF filtered results vs. flow vane measurements (enlarged).

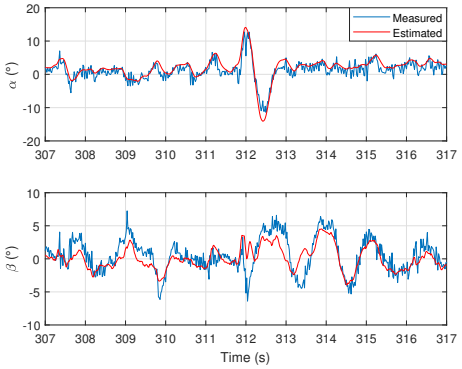

Fig. 12. Phastball CF inertial results vs. flow vane measurements (enlarged).

are used as the ground truth for comparison. It can be seen from the table that the inertial EKF has similar performance compared with the inertial CF for AOA/AOS estimation.

As for KHawk 55" UAV, IMU measurements $[a_x, a_y, a_z, p, q, r]$, airspeed measurement $[V_{pitot}]$, aircraft attitude $[\phi, \theta]$, aircraft lift coefficients $[C_{L_0}, C_{L_\alpha}, C_{L_q}, C_{L_{\delta_e}}]$, and side force coefficients $[C_{Y_0}, C_{Y_\beta}, C_{Y_p}, C_{Y_r}, C_{Y_{\delta_a}}, C_{Y_{\delta_r}}]$ are available. Only two inertial AOA/AOS estimation filters are evaluated because the 5-hole pitot tube has been calibrated by the manufacturer. Flight data were collected during the flight test with aggressive elevator sinusoidal inputs and aileron doublets. The aircraft was close to stall several times during the flight test. Estimated AOA/AOS and 5-Hole pitot tube measured AOA/AOS are shown in Figs. 15-18.

Statistical analysis of estimation results are provided in Table VI. The AOA and AOS measured by the 5-hole pitot tube are used as ground truth for comparison. It can be observed from the table that the CF has similar performance compared with the EKF for inertial AOA/AOS estimation.

In summary, all four filters are effective for flow angle estimation. Two direct flow angle filtering methods are able to increase the reliability of the direct flow angle measurement system. Two inertial filters can work independently or work as a backup for direct flow angle measurement systems. The tuning strategies used in this paper work desirably across platforms. The estimation errors from inertial flow angle esti-

TABLE V
STATISTICAL ANALYSIS OF FILTER ESTIMATION RESULTS USING PHASTBALL DATA

Method	AOA mean error (°)	AOA error std. (°)	AOS mean error (°)	AOS error std. (°)
CF Inertial	1.2031	0.9653	1.4859	1.4953
EKF Inertial	1.4137	1.4144	1.1394	1.6624

TABLE VI
STATISTICAL ANALYSIS OF FILTER ESTIMATION RESULTS USING KHAWK55" DATA

Method	AOA mean error (°)	AOA error std. (°)	AOS mean error (°)	AOS error std. (°)
CF Inertial	1.9640	1.2042	2.0204	2.1768
EKF Inertial	1.8805	1.3643	2.0384	2.1030

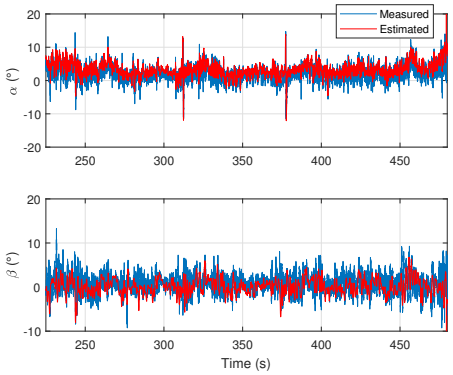

Fig. 13. Phastball EKF inertial results vs. flow vane measurements.

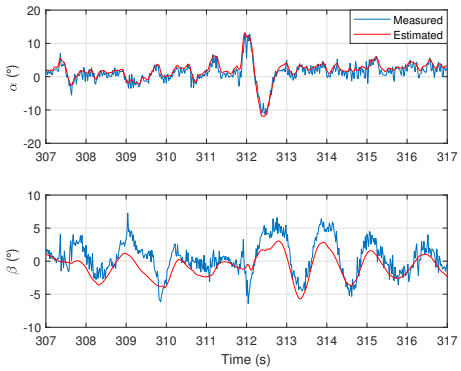

Fig. 14. Phastball EKF inertial results vs. flow vane measurements (enlarged).

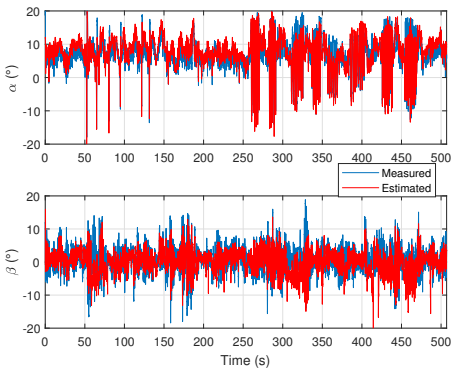

Fig. 15. KHawk 55" CF inertial results vs. 5-hole measurements.

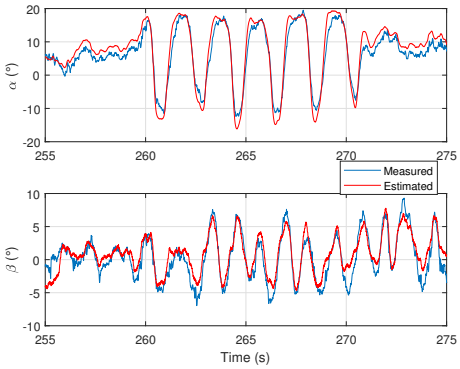

Fig. 16. KHawk 55" CF inertial results vs. 5-hole measurements (enlarged).

mation filters may be caused by sensor alignment errors and uncorrected local flow effects such as upwash and sidewash.

The following suggestions are made based on flight test results. If there are low quality direct flow angle measurements available on UAVs and their major applications are for stall warning or flight control, the flow angle filtering CF is recommended since it is the easiest to implement among the four filters and requires far less tuning than the flow angle filtering EKF. However, if the major applications are for sensor fault detection or dynamic wind estimation, the flow angle filtering EKF is recommended given its flexibility and robustness [15], [50]. When direct flow angle measurements are not available on UAVs, the inertial CF and inertial EKF can be implemented. Similar to the flow angle filtering filters, the inertial CF is recommended for stall warning and flight control, whereas the inertial EKF is recommended for sensor fault detection or prevailing wind estimation. There are also many other applications if a UAV has redundant flow angle information, i.e. direct flow angle measurements and inertial flow angle estimates. Such a UAV platform can be used in areas such as turbulence detection/modeling and aircraft structure damage assessment [8], [38].

VI. CONCLUSIONS & FUTURE WORKS

Four AOA/AOS (flow angle) estimation filters are designed and evaluated on two different UAV platforms, which include

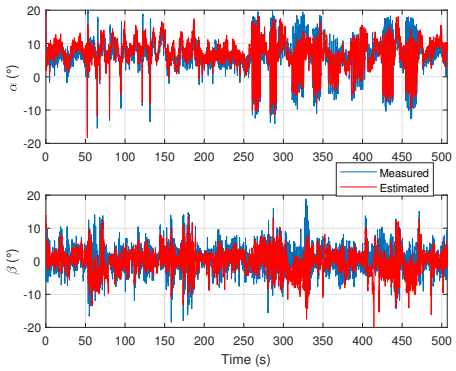

Fig. 17. KHawk 55" EKF inertial results vs. 5-hole measurements.

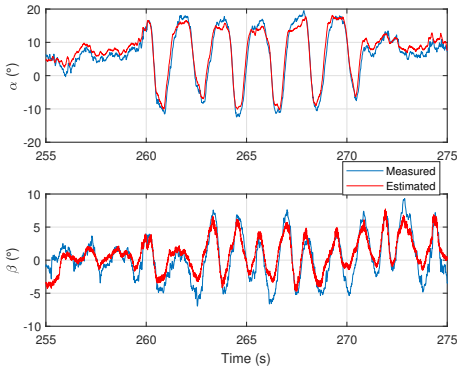

Fig. 18. KHawk 55" EKF inertial results vs. 5-hole measurements (enlarged).

a new CF and a new EKF for inertial AOA/AOS estimation as well as a CF and an EKF for the filtering of direct flow angle measurements. Thorough implementation and tuning process of the filters are introduced in the paper. Detailed analysis and recommendations for different applications are also provided. Simulation results show that all four filters can estimate flow angles accurately compared with the ground truth. For flight test data, the proposed inertial CF and EKF show good performance in estimating flow angles (the root mean square errors are less than 1.5 degrees under nominal flight conditions and around 2 degrees under aggressive maneuvers) compared with direct flow angle measurements from the mechanical vanes or 5-hole pitot tube. It can also be observed that the inertial CF has similar performance with the inertial EKF, while taking less tuning efforts and computational resources. The advantage of the inertial EKF lies in its flexibility in the formulation, which can be easily modified for estimation of other states such as 3D wind. The two flow angle filtering methods show their effectiveness in rejecting high frequency noise when direct flow angle measurements are available. In the future, more cases on the estimation of AOA and AOS will be studied under different dynamic flow fields, such as wake vortices generated by aircraft and turbulence caused by fire. This will greatly help the understanding of the interaction among aircraft, dynamics flow fields, and flight controllers.

ACKNOWLEDGMENTS

This work was partially supported by NASA grant #NNX14AF55A. P. Tian and H. Chao were also partially supported by the University of Kansas General Research Fund allocation #2221800.

REFERENCES

[1] J. D. Anderson Jr, *Fundamentals of aerodynamics*. McGraw-Hill Education, Sixth Edition, 2017.
[2] V. Klein and E. A. Morelli, *Aircraft system identification: theory and practice*. AIAA Education Series, AIAA, Reston, VA, 2006.
[3] R. Jategaonkar, *Flight Vehicle System Identification: A Time Domain Methodology*. AIAA Progress in Astronautics and Aeronautics, AIAA, Reston, VA, 2006, vol. 216.
[4] P. Bala, E. Kupcis, and W. Fisher, "Aircraft stall warning system," Mar. 13 1990, uS Patent 4,908,619. [Online]. Available: https://www.google.com/patents/US4908619
[5] P. Catlin, D. Ballard, G. Watson, and A. Worden, "Aircraft stall warning system," Jan. 21 1997, uS Patent 5,595,357. [Online]. Available: https://www.google.com/patents/US5595357
[6] B. d'Enquetes et d'Analyses, "Final report on the accident on 1st june 2009 to the airbus a330-203 registered f-gzcp operated by air france flight af 447 rio de janeiro–paris," *Paris, France: BEA*, 2012.
[7] K. A. Wise, "Flight testing of the x-45a j-ucas computational alpha-beta system," in *AIAA Guidance, Navigation, and Control Conference and Exhibit*. AIAA Paper 2006-6215, 2006.
[8] D. Fischenberg, "A method to validate wake vortex encounter models from flight test data," in *27th International Congress of the Aeronautical Sciences*. ICAS 2010-6.9.1, 2010.
[9] H. Chao, Y. Gu, P. Tian, Z. C. Zheng, and M. R. Napolitano, "Wake vortex detection with uav close formation flight," in *AIAA Atmospheric Flight Mechanics Conference*. AIAA Paper 2015-2396, 2015.
[10] M. B. Rhudy, Y. Gu, J. N. Gross, and H. Chao, "Onboard wind velocity estimation comparison for unmanned aircraft systems," *IEEE Transactions on Aerospace and Electronic Systems*, vol. 53, no. 1, pp. 55–66, 2017.
[11] W. Gracey, "Summary of methods of measuring angle of attack on aircraft," Langley Aeronautical Laboratory, Tech. Rep., 1958.
[12] E. A. Haering Jr, "Airdata measurement and calibration," NASA, Tech. Rep., 1995.
[13] ——, "Airdata calibration of a high-performance aircraft for measuring atmospheric wind profiles," NASA, Tech. Rep., 1990.
[14] E. A. Morelli, "Real-time aerodynamic parameter estimation without air flow angle measurements," *Journal of Aircraft*, vol. 49, no. 4, pp. 1064–1074, 2012.
[15] M. B. Rhudy, T. Larrabee, H. Chao, Y. Gu, and M. Napolitano, "Uav attitude, heading, and wind estimation using gps/ins and an air data system," in *AIAA Guidance, Navigation, and Control Conference*. AIAA Paper 2013-5201, 2013.
[16] T. Berger, M. Tischler, S. G. Hagerott, D. Gangsaas, and N. Saeed, "Longitudinal control law design and handling qualities optimization for a business jet flight control system," in *AIAA Atmospheric Flight Mechanics Conference*. AIAA Paper 2012-4503, 2012.
[17] ——, "Lateral/directional control law design and handling qualities optimization for a business jet flight control system," in *AIAA Atmospheric Flight Mechanics Conference*. AIAA Paper 2013-4506, 2013.
[18] R. P. Quinlivan, "Aircraft angle-of-attack and sideslip estimator," Sep. 6 1977, uS Patent 4,046,341. [Online]. Available: https://www.google.com/patents/US4046341
[19] J. E. Zeis, "Angle of attack and sideslip estimation using an inertial reference platform," Master Thesis, Air Force Institute of Technology, 1988.
[20] R. D. Colgren, "Method and system for estimation and correction of angle-of-attack and sideslip angle from acceleration measurements," Aug. 14 2001, uS Patent 6,273,370. [Online]. Available: https://www.google.com/patents/US6273370
[21] N. Shantha Kumar and G. Girija, "Filtering and fusion based reconstruction of angle of attack," in *National Conference on Range Technology*, 2006.
[22] S. Myschik, F. Holzapfel, and G. Sachs, "Low-cost sensor based integrated airdata and navigation system for general aviation aircraft," in *Proceedings of AIAA Guidance, Navigation, and Control Conference and Exhibit*, 2008.

[23] J. Perry, A. Mohamed, B. Johnson, and R. Lind, "Estimating angle of attack and sideslip under high dynamics on small uavs," in *ION GNSS Conference*, 2008, pp. 16–19.
[24] C. Ramprasadh and H. Arya, "Multistage-fusion algorithm for estimation of aerodynamic angles in mini aerial vehicle," *Journal of Aircraft*, vol. 49, no. 1, pp. 93–100, 2012.
[25] A. Cho, Y.-s. Kang, B.-j. Park, and C.-s. Yoo, "Airflow angle and wind estimation using gps/ins navigation data and airspeed," in *Control, Automation and Systems (ICCAS), 2013 13th International Conference on*. IEEE, 2013, pp. 1321–1324.
[26] F. A. P. Lie and D. Gebre-Egziabher, "Synthetic air data system," *Journal of Aircraft*, vol. 50, no. 4, pp. 1234–1249, 2013.
[27] T. A. Johansen, A. Cristofaro, K. Sørensen, J. M. Hansen, and T. I. Fossen, "On estimation of wind velocity, angle-of-attack and sideslip angle of small uavs using standard sensors," in *Unmanned Aircraft Systems (ICUAS), 2015 International Conference on*. IEEE, 2015, pp. 510–519.
[28] A. Wenz, T. A. Johansen, and A. Cristofaro, "Combining model-free and model-based angle of attack estimation for small fixed-wing uavs using a standard sensor suite," in *International Conference on Unmanned Aircraft Systems*. IEEE, 2016, pp. 624–632.
[29] M. Heller, S. Myschik, F. Holzapfel, and G. Sachs, "Low-cost approach based on navigation data for determining angles of attack and sideslip for small aircraft," in *AIAA Guidance, Navigation, and Control Conference and Exhibit*. AIAA Paper 2003-5777, 2003.
[30] A. Cho, J. Kim, S. Lee, and C. Kee, "Wind estimation and airspeed calibration using a uav with a single-antenna gps receiver and pitot tube," *IEEE transactions on aerospace and electronic systems*, vol. 47, no. 1, pp. 109–117, 2011.
[31] P. Tian, H. Chao, Y. Gu, and S. G. Hagerott, "Uav flight test evaluation of fusion algorithms for estimation of angle of attack and sideslip angle," in *AIAA Guidance, Navigation, and Control Conference*. AIAA Paper 2016-0645, 2016.
[32] NASA. (2015) Inclination effects on lift. [Online]. Available: https://www.grc.nasa.gov/www/k-12/airplane/incline.html
[33] F. R. David. (2015) Absolute angle of attack. [Online]. Available: http://www.nar-associates.com/technical-flying/angle_of_attack /absolute_wide_screen.pdf
[34] Wikipedia. (2017) Slip (aerodynamics). [Online]. Available: https://en.wikipedia.org/wiki/Slip_(aerodynamics)
[35] B. Martos and D. F. Rogers, "Low cost accurate angle of attack system," in *55th AIAA Aerospace Sciences Meeting*. AIAA Paper 2017-1215, 2017.
[36] S. A. Whitmore, R. J. Davis, and J. Fife, "In-flight demonstration of a real-time flush airdata sensing system," *Journal of aircraft*, vol. 33, no. 5, pp. 970–977, 1996.
[37] T. K. McDevitt and F. K. Owen, "An optical angle of attack sensor," in *International Congress on Instrumentation in Aerospace Simulation Facilities*. IEEE, 1989, pp. 113–124.
[38] P. Tian, A. He, H. Chao, Z. C. Zheng, and Y. Gu, "Wake encounter simulation and flight validation with uav close formation flight," in *AIAA Guidance, Navigation, and Control Conference*. AIAA Paper 2017-1910, 2017.
[39] J. L. Crassidis, F. L. Markley, and Y. Cheng, "Survey of nonlinear attitude estimation methods," *Journal of Guidance, Control, and Dynamics*, vol. 30, no. 1, pp. 12–28, 2007.
[40] J. N. Gross, Y. Gu, M. B. Rhudy, S. Gururajan, and M. R. Napolitano, "Flight-test evaluation of sensor fusion algorithms for attitude estimation," *IEEE Transactions on Aerospace and Electronic Systems*, vol. 48, no. 3, pp. 2128–2139, 2012.
[41] G. Bishop and G. Welch, "An introduction to the kalman filter," *Proc of SIGGRAPH, Course*, vol. 8, no. 27599-23175, p. 41, 2001.
[42] M. R. Napolitano, H. Chao, Y. Gu, C. E. Hanson, and M. T. Stanley, "Cooperative gust sensing and suppression for aircraft formation flight," NASA LEARN Project Phase I, Final Report, Tech. Rep., 2014.
[43] M. Rhudy, J. Gross, Y. Gu, and M. Napolitano, "Fusion of gps and redundant imu data for attitude estimation," in *AIAA Guidance, Navigation, and Control Conference*. AIAA Paper 2012-5030, 2012.
[44] Y. Gu, S. Gururajan, B. Seanor, H. Chao, and M. R. Napolitano, "Building better tools: Experimental uav research at west virginia university," in *American Control Conference*. IEEE, 2013, pp. 1454–1459.
[45] MicroStrain, *3DM-GX3®-25 Datasheets*, LORD Corporation, 2014.
[46] A. K. McGrail, "Onboard parameter identification for a small uav," Master Thesis, West Virginia University, 2012.
[47] H. Chao, H. P. Flanagan, P. Tian, and S. G. Hagerott, "Flight test investigation of stall/spin detection techniques for a flying wing uas," in *AIAA Atmospheric Flight Mechanics Conference*. AIAA Paper 2017-1631, 2017.
[48] MicroStrain, *3DM-GX3®-25 Data Communications Protocol*, MicroStrain Inc., 2011.
[49] W. Gracey, "Measurement of aircraft speed and altitude," Langley Research Center, Tech. Rep., 1980.
[50] L. Van Eykeren and Q. Chu, "Sensor fault detection and isolation for aircraft control systems by kinematic relations," *Control Engineering Practice*, vol. 31, pp. 200–210, 2014.